BNL-111872-2016-TECH
EIC/51;BNL-111872-2016-IR

# An electron storage ring proposal for the Ring-Ring eRHIC project

S. Tepikian

February 2016

Collider Accelerator Department
**Brookhaven National Laboratory**

**U.S. Department of Energy**
USDOE Office of Science (SC), Nuclear Physics (NP) (SC-26)

# DISCLAIMER

BNL-111872-2016-IR

eRHIC/51
February 2016

# An electron storage ring proposal for the Ring-Ring eRHIC project

**S. Tepikian, M. Blaskiewicz, C. Montag, S. Peggs**

**Collider-Accelerator Department**
**Brookhaven National Laboratory**
**Upton, NY 11973**

**U.S. Department of Energy**
**Office of Science, Office of Nuclear Physics**

# An Electron Storage Ring Proposal for the Ring-Ring eRHIC Project

S. Tepikian, M. Blaskiewicz, C. Montag, S. Peggs

A design of the Ring-Ring eRHIC electron storage ring is proposed. This design will cover three energy configurations denoted as *Low*, *Middle* and *High*. The requirements for this ring are defined in the baseline Table 1. This ring must fit in the existing RHIC tunnel and the circumference has to match that of RHIC.

| | **Low** | **Middle** | **High** |
|---|---|---|---|
| **Energy [GeV]** | 5 | 20 | 20 |
| **Magnetic Rigidity: Bρ [T-m]** | 16.6782 | 66.7128 | 66.7128 |
| **Bunch Population [$10^{11}$]** | 2.08 | 1.14 | 1.14 |
| **Number of Bunches** | 360 | 360 | 360 |
| **Beam Current [A]** | 0.925 | 0.508 | 0.508 |
| **Energy loss per turn: $U_0$ [MeV]** | 0.18 | 47.1 | 47.1 |
| **Arc SR Power: $P_{arc}$ [MW]** | 0.2 | 23.9 | 23.9 |
| **Emittance: $\varepsilon_H$, $\varepsilon_V$ [nm]** | 106.0, 19.0 | 62.2, 11.2 | 53.0, 9.5 |
| **IP betas: $\beta_H$, $\beta_V$ [m]** | 0.86, 0.60 | 0.61, 0.42 | 0.38, 0.27 |

*Table 1: The baseline design goals for the electron storage ring [1].*

The ring is designed to be modular consisting of: (1) arc cells, (2) dispersion suppressors, (3) three straight sections without dispersion, (4) a straight section with dispersion which includes a Robinson Wiggler [2] to control the emittance in the low energy configuration and (5) two low-β IRs that can operate in both colliding and non-colliding mode. The following sections discuss these different beam line sections.

## Cell Choice

There are many cell configurations available that are used in electron storage rings [2][3]. Their goal is to achieve a low emittance. But, this often leads to a low packing factor for the dipoles. A basic rule of thumb is, the lower the packing factor, the lower the emittance that can be achieved. Since, a high packing factor leads to longer dipoles, thus, lower dipole field and in turn lower electron radiation – for high energy operation – this reduces operational cost. Furthermore, moderate emittances are required for the baseline. Three cell types given below are considered:

1. FODO cell. A standard cell structure shown in Fig 1.
2. TBA cell. Triple Bend Achromat shown in Fig 2.
3. TAL cell. Triplet Achromat Lattice shown in Fig 3.

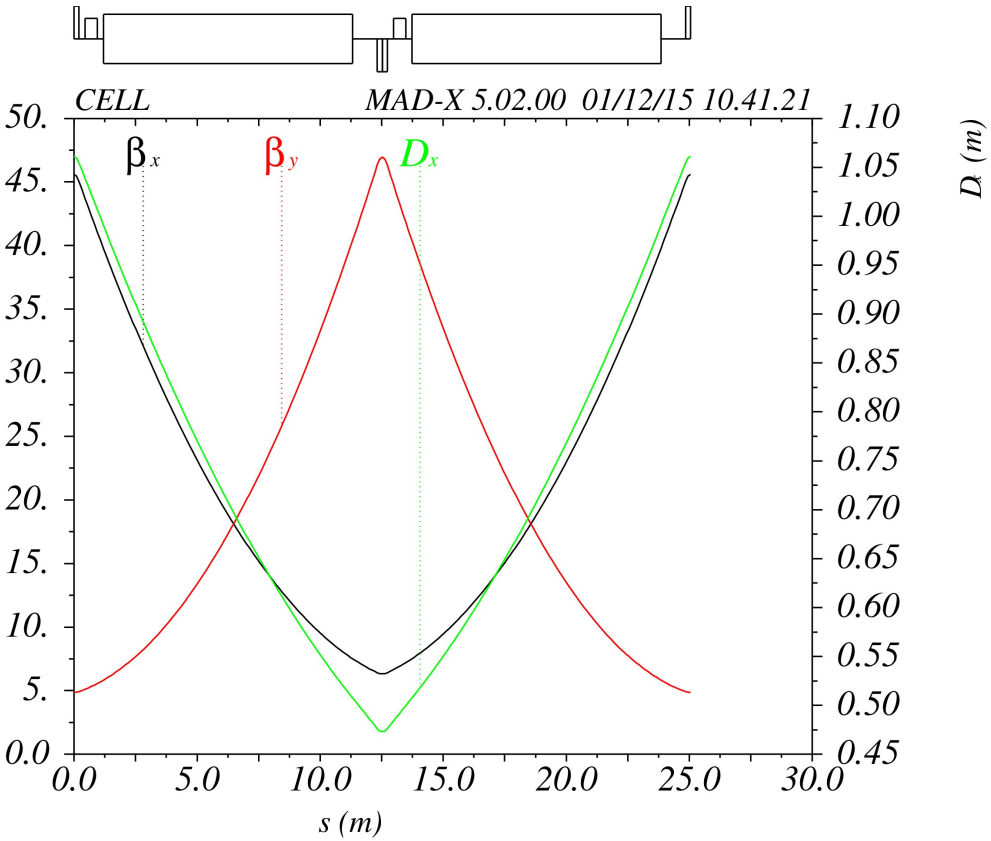


*Figure 1: A standard FODO cell.*

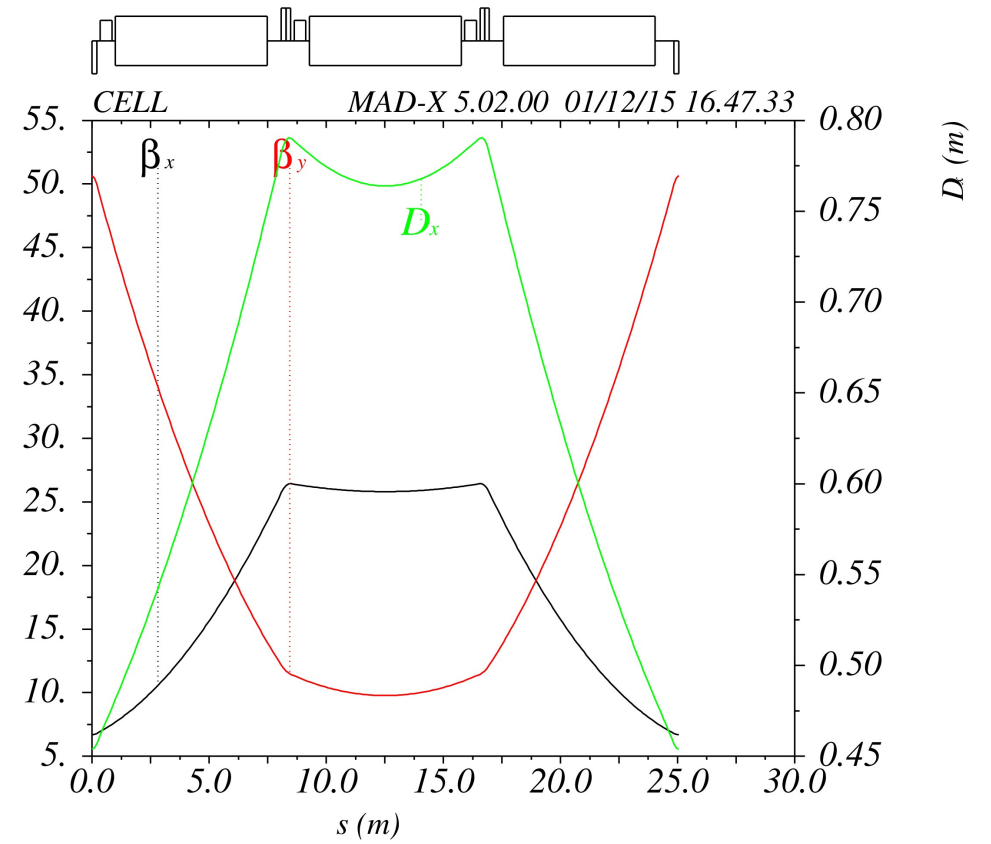


*Figure 2: Triple Bend Achromat (TBA) cell.*

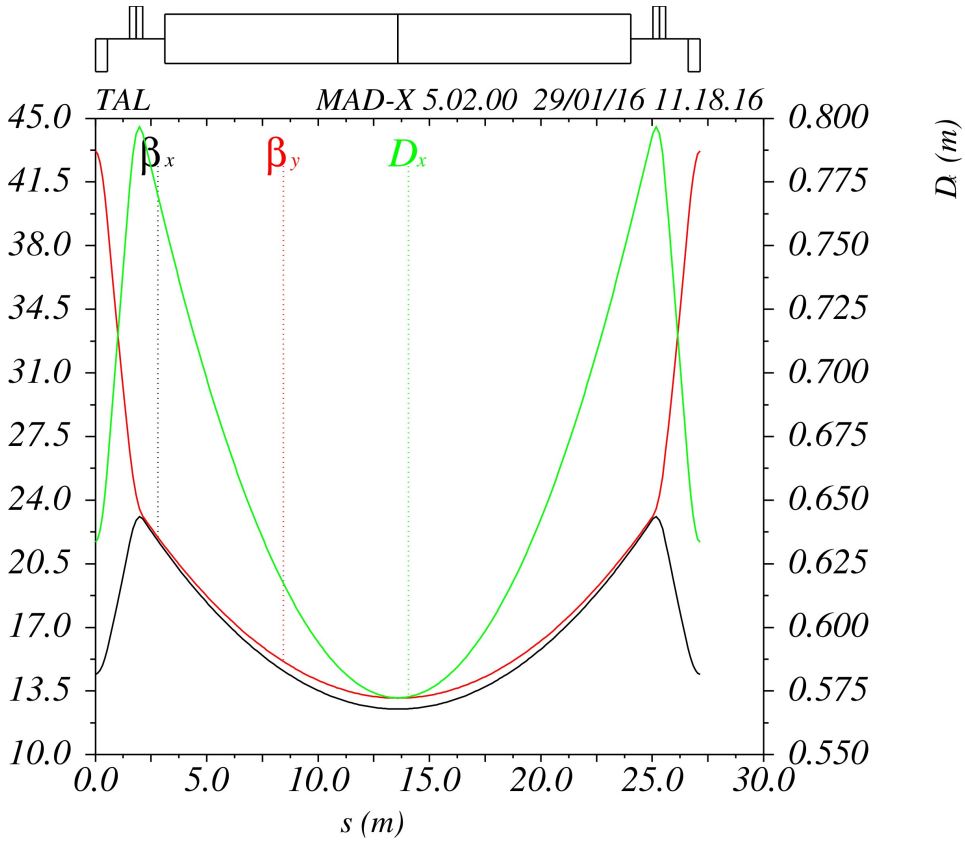


*Figure 3: Triplet Achromat Lattice (TAL) cell.*

The TAL cell loses out for two reasons. The quadrupole strengths are higher than the other cells require, thus longer quadrupoles are needed, reducing the packing factor. Furthermore, the chromatic correction becomes more difficult with this cell.

Next, the TBA cell shows a lot of promise and a full ring was designed with this cell. In order to reduce the packing factor, the drift spaces between the magnets were reduced. This adds a constraint if we wish to use existing quadrupoles such as those available from PEP II [4]. Furthermore, the lower dispersion leads to stronger sextupoles for chromatic correction and larger higher-order chromatic effects.

Finally, the FODO cell gives the highest packing factor and has the space to use the longer PEP II quadrupoles. The requested baseline emittances are achievable with this cell. The higher order chromatic effects are reasonable with two families of sextupoles. Final results are shown in Table 5.

Tables 2-4 shows the horizontal cell phase advance at various energies and cell lengths to get an emittance of 53 nm. The TAL cell has significantly lower dipole bending radius, ρ, which will lead to high power requirements, which is more than the baseline parameters. The TBA cell has more moderate dipole bending radius, but may still have some difficulty in reaching the baseline power requirements. The FODO cell which has dipoles with the longest bending radius will be able to meet the baseline power requirements and achieve the emittance requirements as well. For these reasons, the FODO cell has been chosen. The 2.4 m space – in the FODO cell – between the dipoles gives enough room to use the existing PEP II quadrupoles.

**FODO Cell**

| | | | | | Horizontal Phase Advance at 53 nm [°] | | | |
|---|---|---|---|---|---|---|---|---|
| $N_{cells}$ | $L_{cell}$ [m] | $L_D$ [m] | ρ [m] | PF [%] | 5 GeV | 10 GeV | 15 GeV | 20 GeV |
| 16 | 27.8166 | 11.5083 | 307.7095 | 72.4011 | 41.6609 | 66.7309 | 89.2446 | 113.0798 |
| 17 | 26.1803 | 10.6902 | 306.2509 | 72.0579 | 39.0228 | 62.3768 | 83.0294 | 103.6440 |
| 18 | 24.7259 | 9.9629 | 304.4450 | 71.6330 | 36.7232 | 58.6099 | 77.7638 | 96.2944 |
| 19 | 23.4245 | 9.3123 | 302.3468 | 71.1393 | 34.7012 | 55.3159 | 73.2226 | 90.2180 |
| 20 | 22.2533 | 8.7266 | 300.0000 | 70.5871 | 32.9096 | 52.4095 | 69.2544 | 85.0392 |
| 21 | 21.1936 | 8.1968 | 297.4402 | 69.9848 | 31.3115 | 49.8256 | 65.7512 | 80.5409 |
| 22 | 20.2303 | 7.7151 | 294.6964 | 69.3392 | 29.8774 | 47.5130 | 62.6328 | 76.5813 |

*Table 2: Horizontal FODO cell phase advance in degrees for different cell lengths at various energies in an arc with a length of 445.06585 m and total bend angle of 60° including dispersion suppressors at the ends.*

**TBA Cell**

| | | | | | Horizontal Phase Advance at 53 nm [°] | | | |
|---|---|---|---|---|---|---|---|---|
| $N_{cells}$ | $L_{cell}$ [m] | $L_D$ [m] | ρ [m] | PF [%] | 5 GeV | 10 GeV | 15 GeV | 20 GeV |
| 16 | 27.8166 | 7.4055 | 297.0143 | 69.8846 | 41.9471 | 66.9532 | 88.9205 | 110.7265 |
| 17 | 26.1803 | 6.8601 | 294.7917 | 69.3617 | 39.3400 | 62.7070 | 83.0356 | 102.5534 |
| 18 | 24.7259 | 6.3753 | 292.2219 | 68.7570 | 37.0671 | 59.0228 | 77.9963 | 95.8703 |
| 19 | 23.4245 | 5.9415 | 289.3597 | 68.0836 | 35.0687 | 55.7951 | 73.6200 | 90.2112 |
| 20 | 22.2533 | 5.5511 | 286.2490 | 67.3517 | 33.2984 | 52.9438 | 69.7781 | 85.3198 |
| 21 | 21.1936 | 5.1979 | 282.9252 | 66.5696 | 31.7200 | 50.4071 | 66.3758 | 81.0324 |
| 22 | 20.2303 | 4.8768 | 279.4175 | 65.7443 | 30.3046 | 48.1364 | 63.3406 | 77.2353 |

*Table 3: Horizontal TBA cell phase advance in degrees for different cell lengths at various energies in an arc with a length of 445.06585 m and total bend angle of 60° including dispersion suppressors at the ends.*

**TAL Cell**

| | | | | | Horizontal Phase Advance at 53 nm [°] | | | |
|---|---|---|---|---|---|---|---|---|
| $N_{cells}$ | $L_{cell}$ [m] | $L_D$ [m] | ρ [m] | PF [%] | 5 GeV | 10 GeV | 15 GeV | 20 GeV |
| 16 | 27.8166 | 21.5776 | 288.4715 | 67.8746 | 41.6390 | 65.4730 | 85.1787 | 102.7059 |
| 17 | 26.1803 | 19.9413 | 285.6387 | 67.2081 | 39.1500 | 61.5768 | 80.0981 | 96.4632 |
| 18 | 24.7259 | 18.4869 | 282.4587 | 66.4598 | 36.9780 | 58.1780 | 75.6810 | 91.0936 |
| 19 | 23.4245 | 17.1855 | 278.9863 | 65.6428 | 35.0673 | 55.1882 | 71.8030 | 86.4085 |
| 20 | 22.2533 | 16.0143 | 275.2654 | 64.7673 | 33.3749 | 52.5394 | 68.3711 | 82.2777 |
| 21 | 21.1936 | 14.9546 | 271.3314 | 63.8417 | 31.8665 | 50.1782 | 65.3135 | 78.6057 |
| 22 | 20.2303 | 13.9913 | 267.2135 | 62.8728 | 30.5150 | 48.0618 | 62.5736 | 75.3201 |

*Table 4: Horizontal TAL cell phase advance in degrees for different cell lengths at various energies in an arc with a length of 445.06585 m and total bend angle of 60° including dispersion suppressors at the ends.*

# Dispersion Suppressor

The dispersion suppressor, denoted as DS, consists of three cells at both ends of each ARC. Thus, the ARC contains all the bending in the ring. A general DS is shown in Fig. 4.

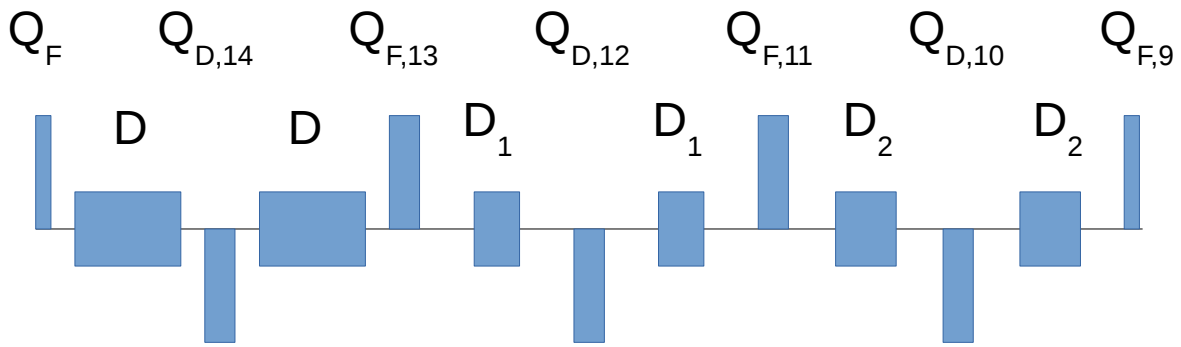


*Figure 4: Basic dispersion suppressor made of three FODO cells. The lengths of the dipoles $D_1$ and $D_2$ are adjusted till the dispersion and its derivative are zero after $Q_{F,9}$. Note, the dipole lengths depends on the horizontal phase advance of the FODO cell. The quadrupoles $Q_{D,14}$ through $Q_{F,9}$ are adjustable for the cases when the horizontal phase advance is different.*

The DS depends on the horizontal phase advance of the cell. From Fig. 4, the regular cell dipole is denoted with, D, and the additional dipoles: $D_1$ and $D_2$ are for the dispersion suppression. The bending angle of the dipoles $D_1$ and $D_2$ are determined from [5] as:

$$\lambda = \frac{1}{4\sin^2(\mu/2)} \qquad \theta_1 = (1-\lambda)\theta \qquad \theta_2 = \lambda\theta$$

where μ is the horizontal phase advance of the cell, $\theta_1$ is the bending angle of dipole $D_1$, $\theta_2$ is the bending angle of dipole $D_2$ and θ is the bending angle of dipole D. This formula also works for the TBA and TAL cells as well. For cells whose phase advance differs from μ, six quadrupoles are adjusted to keep the dispersion suppressed and have the same cell Twiss parameters (six constraints) at the end of the DS. Note, when the quadrupoles are changed their corresponding Twiss parameters will no longer be cell-like within the DS. Some of the beta functions can become quite large, so the choice of μ is important. For this ring after a few tries, we settled on μ=60° horizontal phase advance. Thus, $D_1$ becomes empty and $D_2$=D. Figs. 5-7 show the final results for the three energy configurations.

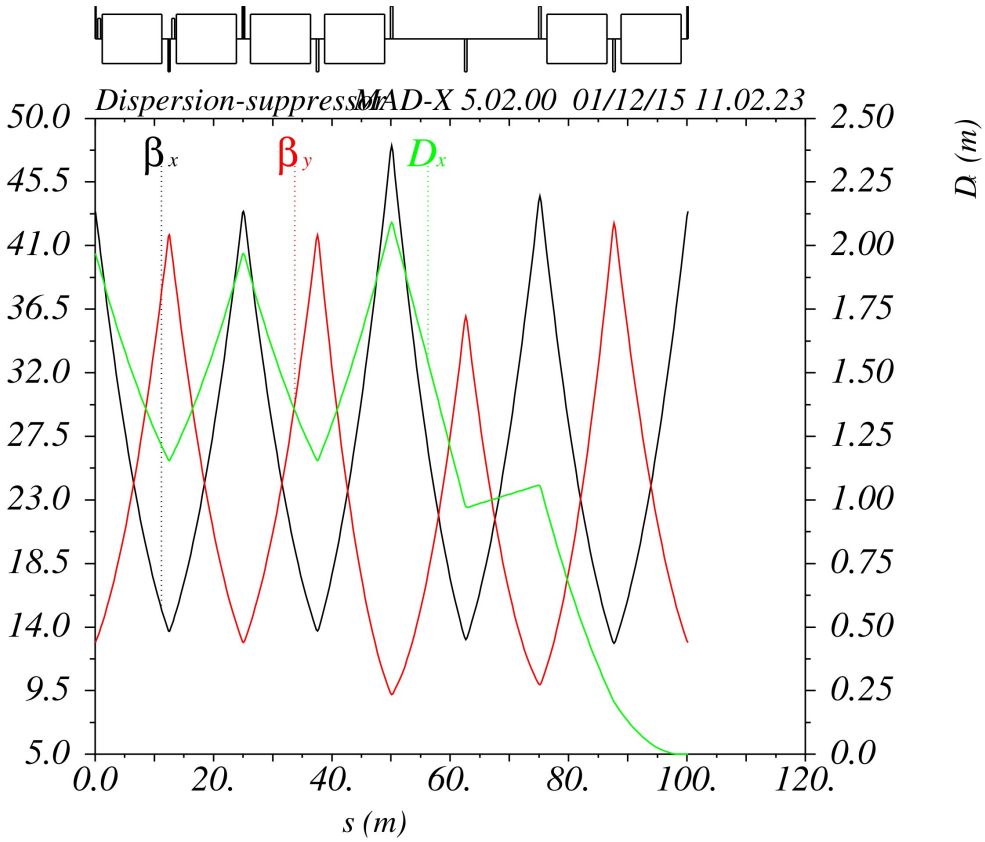


*Figure 5: Dispersion suppressor for the low energy configuration. Cell horizontal phase advance is about 61.76°.*

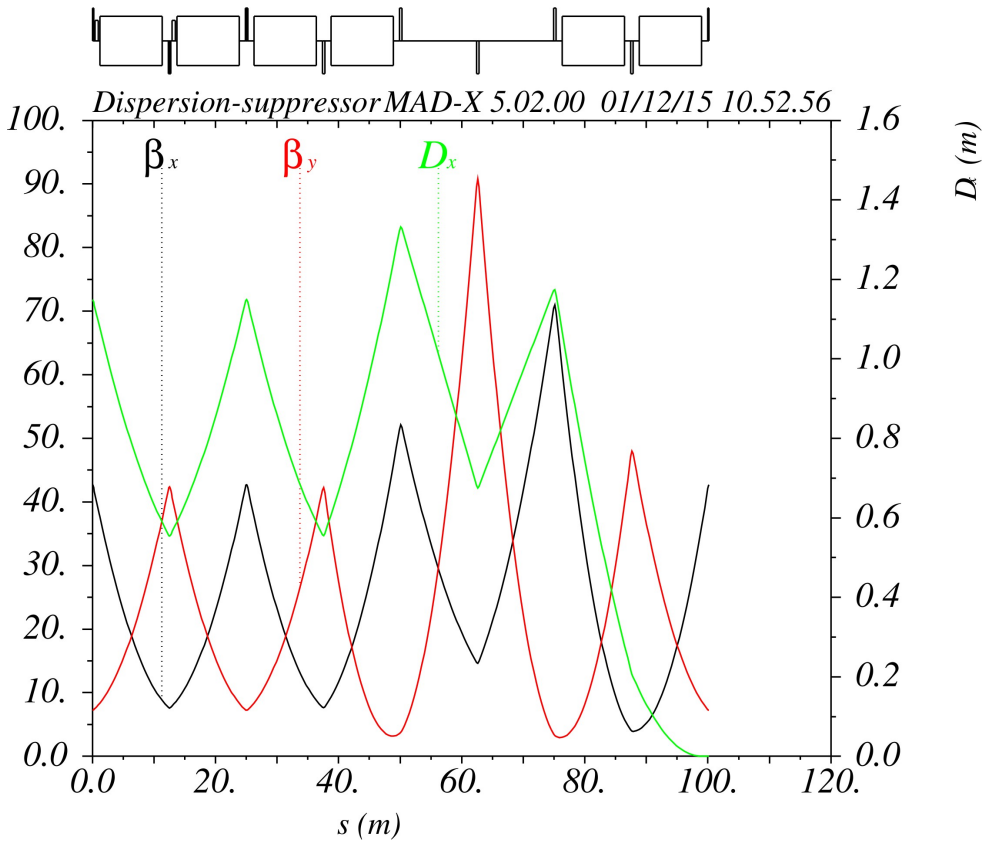


*Figure 6: Dispersion suppressor for the middle energy configuration. Cell horizontal phase advance is about 88.06°.*

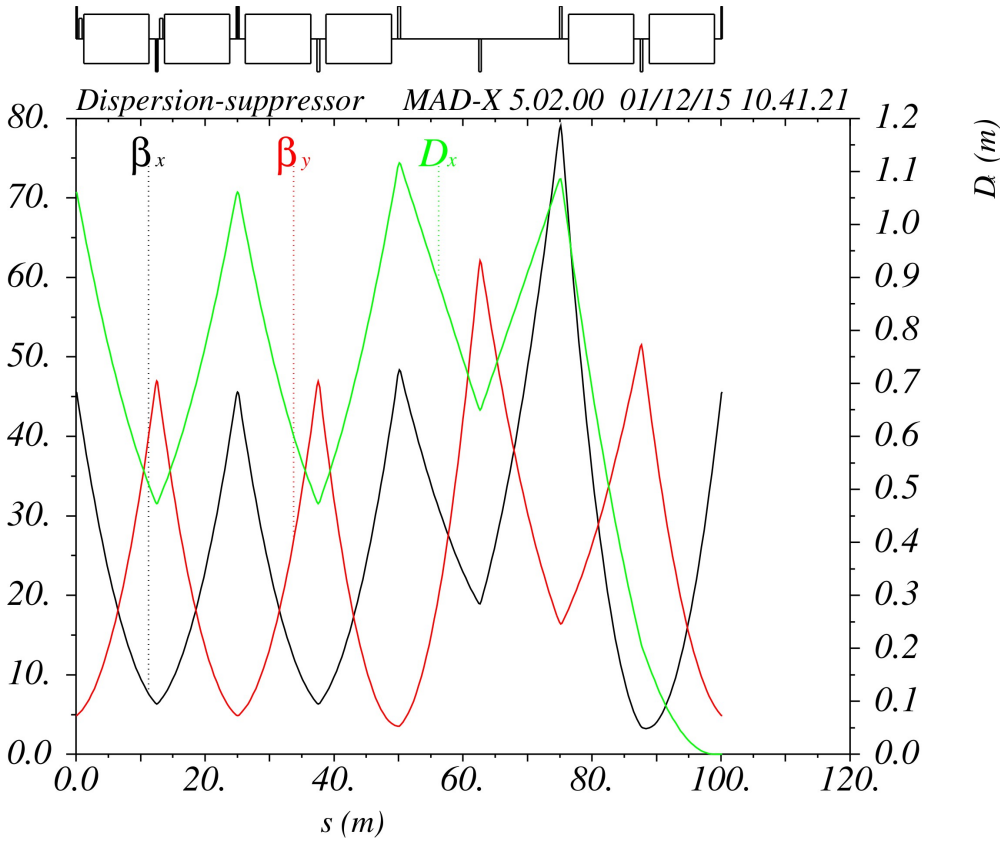


*Figure 7: Dispersion suppressor for the high energy configuration. Cell horizontal phase advance is about 95.07°.*

# ARC

The arc consists of 12 FODO cells plus two DSs (3 cells per DS) at each end[1]. The ring consists of 6 ARCs with straight sections between them. The total bending angle of the ARC must be 60°=360°/6. The total circumference of the ring is set to 3833.845181 m to match the RHIC ring. Finally, the length of the ARC, 450.857709 m, is determined such that the IP points of this ring match the IP points of RHIC. Thus, the lengths of the straight sections between the ARCs is determined to be 188.116488 m. Fig. 8 shows the ARC for the high energy configuration.

There are 18=3+12+3 cells needed per arc. Thus, each cell has a length of 25.047651 m. Since, the space allocated for the quadrupoles, BPMs, correctors, sextupoles, etc, is 2.4 m between the dipoles, the dipole length is 10.123825 m. Taking into account the DSs, there are 32 dipoles per ARC. This leads to a dipole bending radius of ρ=309.361304 m.

1 There is one straight section that has dispersion present. In this case the DSs about this straight section are replaced by three cells where the last cell has no dipoles.

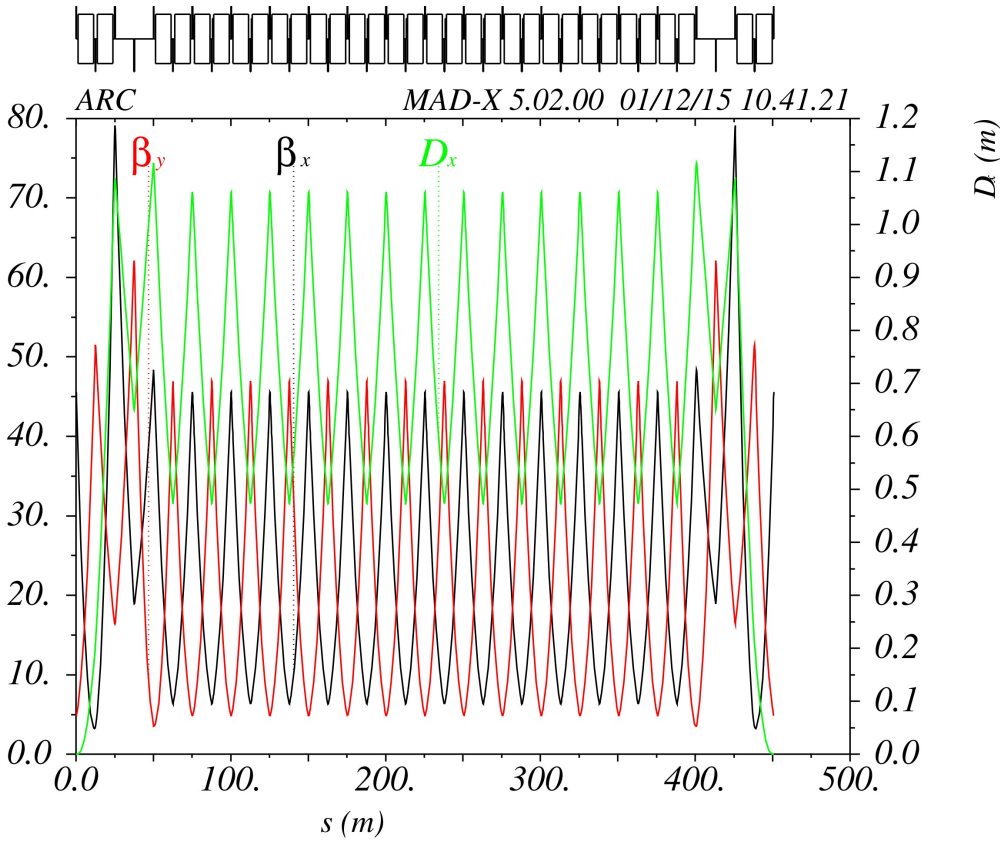


*Figure 8: One of six ARCs in the ring for the high energy configuration.*

# Colliding IP (Dispersion Free)

Two of the straights will have optics for colliding the electron beam with beam in the RHIC ring. The optics for these sections are symmetric. Each energy configuration has different $\beta^*$ at the collision point (IP), see Table 1. The high energy configuration has the smallest $\beta^*$=(0.38 m, 0.27 m) at the IP and largest $\beta_{max}$=604 m. These sections can also be set to non-colliding mode with a larger $\beta^*$ at the IP and a smaller $\beta_{max}$. This section includes a large empty drift space of 35 m long for spin rotators and other devices as needed. Fig. 9-10 shows the optics for this section in both high energy colliding mode and non-colliding mode respectively.

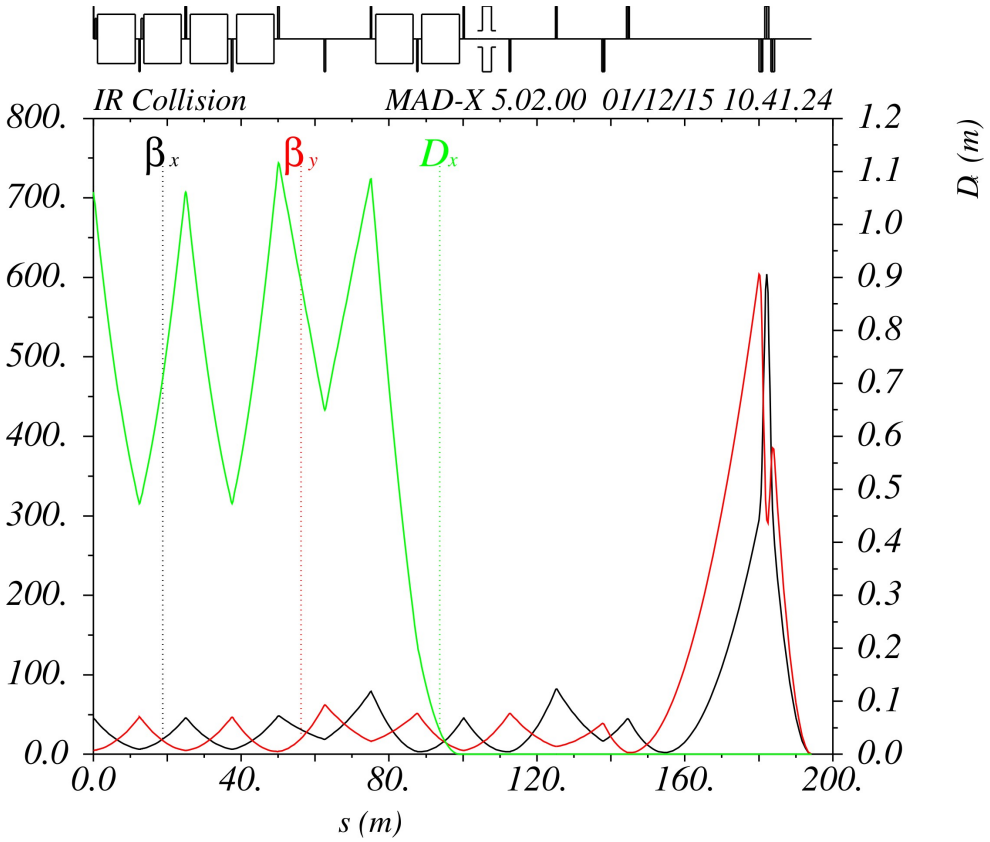


*Figure 9: The optics for the colliding section in colliding mode for the high energy configuration.*

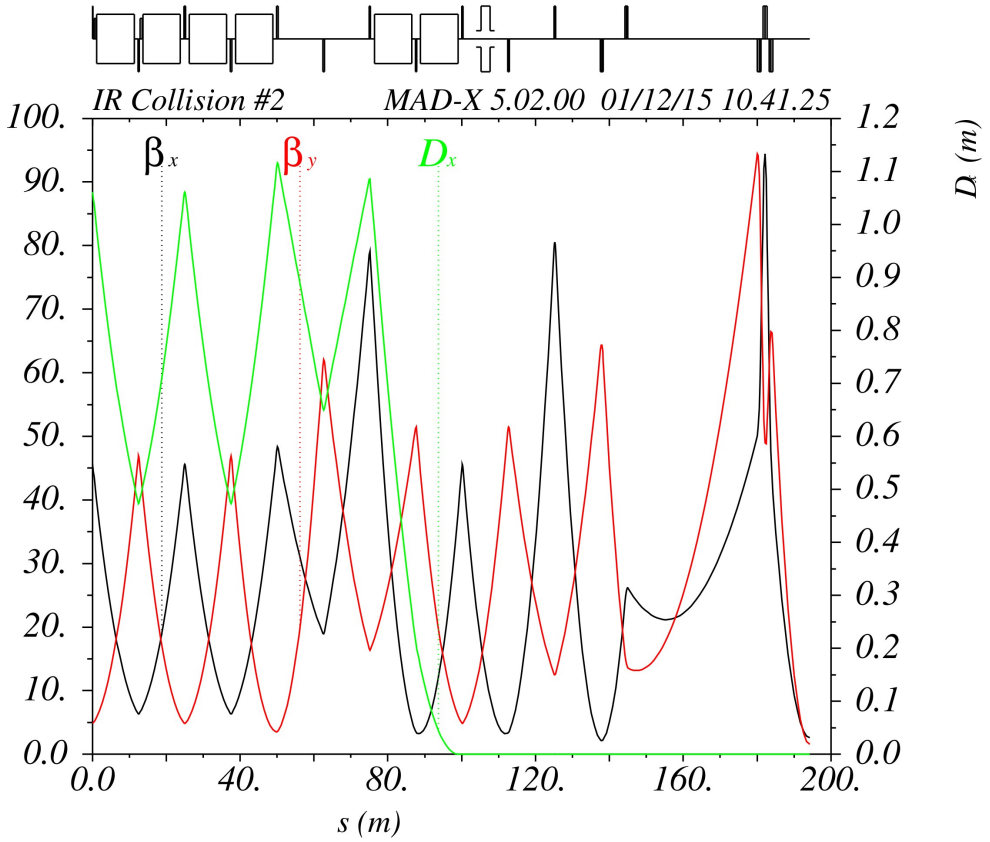


*Figure 10: The optics for the colliding sector in the non-colliding mode.*

# Non-Colliding Section (Dispersion Free)

Three straight sections are non-colliding sections without dispersion. The $\beta_{max}$ are kept small in this section. Additional families of sextupoles can be added to correct for amplitude dependent tunes. Empty drift spaces are available for other equipment that can be added as well. Fig. 11 shows this section from the high energy configuration.

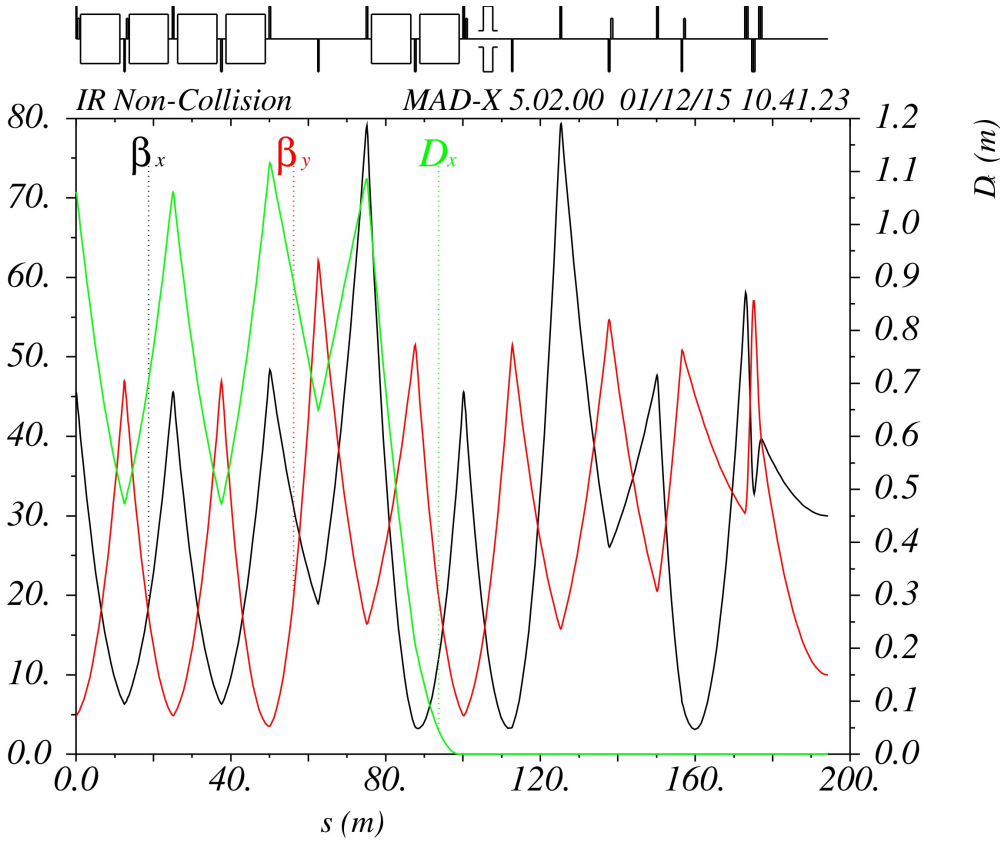


*Figure 11: The dispersion free non-colliding section. There are three of these in the ring.*

# Non-Colliding Section (with Dispersion)

There is one straight section that includes dispersion. The main purpose of this section is to include the Robinson Wiggler [2], denoted as RW, to control the emittance in the low energy configuration. The goal emittance at low energy is 106 nm (5 GeV), compared to high energy 53 nm (20 GeV). Taking into account that the emittance changes as the square of the energy, the low energy emittance reduces by factor of 16. Furthermore, the emittance requirement increases by a factor of 2. Thus, the low energy configuration needs to be increased by a factor 32 over the high energy configuration. To achieve this, we reduce the horizontal phase advance of the cell to about 60°[2] from the high energy configuration giving us about a factor 3 increase in emittance. To get an additional factor of 10 required, a RW is employed. The RW consists of 4 dipoles with gradients, see Fig. 12. The RW changes the damping partition number, denoted as $\mathcal{D}$, as:

2 Choosing a phase advance lower than 60° would require negative bends for the dispersion suppressor.

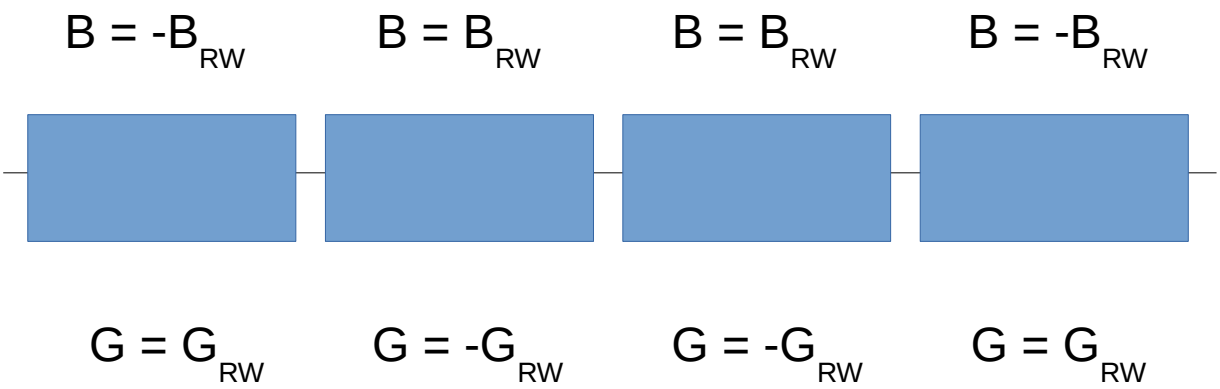


*Figure 12: A schematic of a Robinson Wiggler. For the RW used in the ring, $L_{RW}$=7.0 m, $\rho_{RW}$=170.0 m, $B_{RW}$=0.09807 T and $G_{RW}=dB_{RW}/dx$=0.3919 T/m.*

$$\Delta \mathcal{D} = \langle \eta \rangle \frac{1}{B_{RW}} \frac{dB_{RW}}{dx} \frac{4 L_{RW} \rho}{2 \pi \rho_{RW}^2} \left( 1 + \frac{4 L_{RW} \rho}{2 \pi \rho_{RW}^2} \right)$$

where $<\eta>$ is the averaged dispersion through the RW, $B_{RW}$, $L_{RW}$, $\rho_{RW}$ and $dB_{RW}/dx$ are the dipole field, length, bending radius and gradient of a RW magnet, $\rho$ is the bending radius of the ARC dipole magnets. Note, for positive dispersion – the damping partition number is increased – which decreases the emittance, however, when the dispersion is negative, the emittance is increased. Figs. 13-15 show the optics of the low, middle and high energy configuration through half the RW respectively.

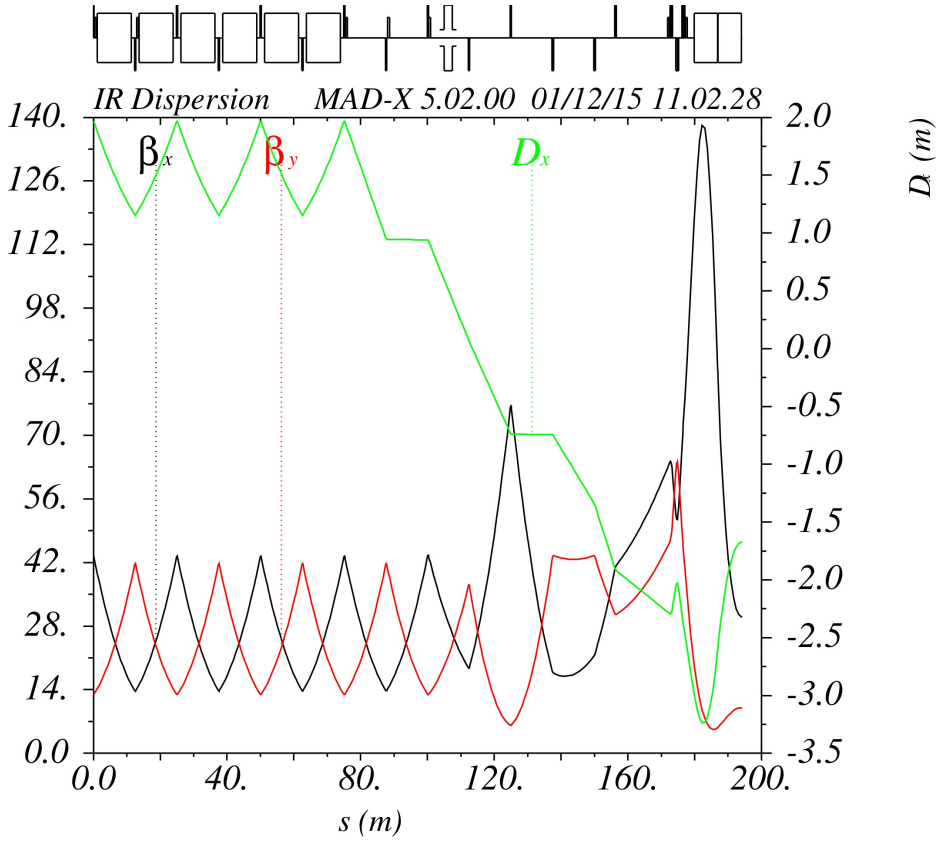


*Figure 13: The straight section with 1/2 of the RW. The optics for the low energy configuration with the RW on. The RW is included when matching to the ARCS. Note the large β-functon through the RW.*

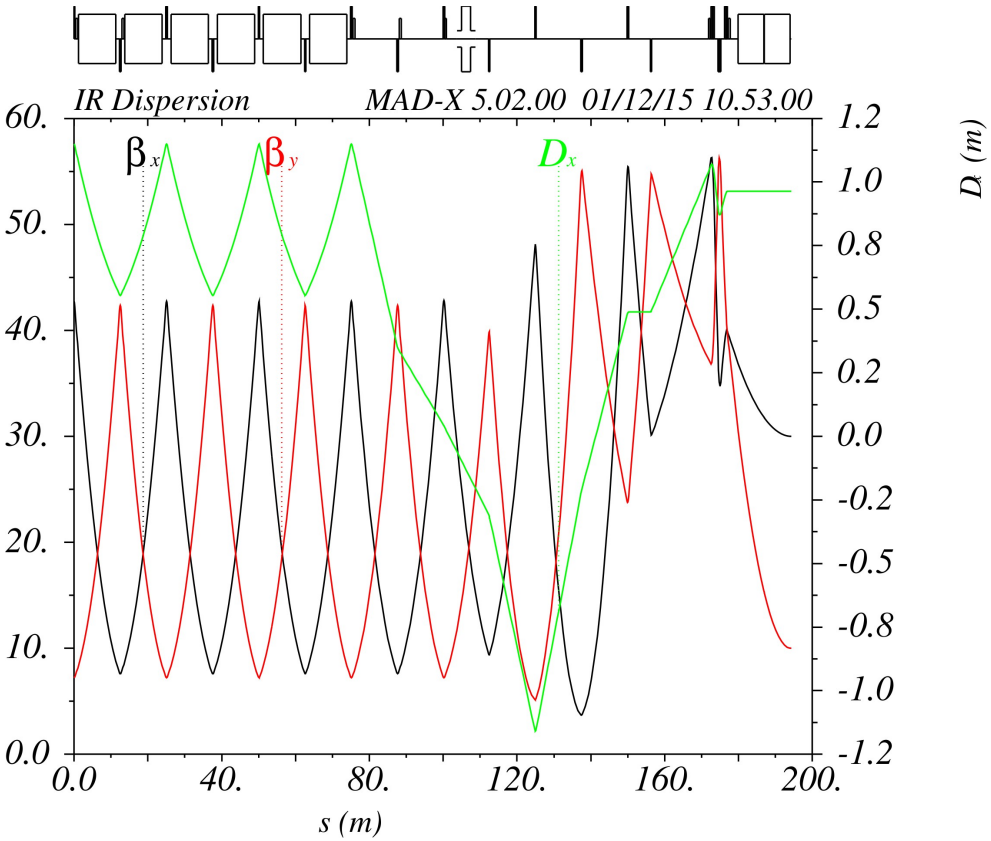


*Figure 14: The middle energy configuration. The RW is off.*

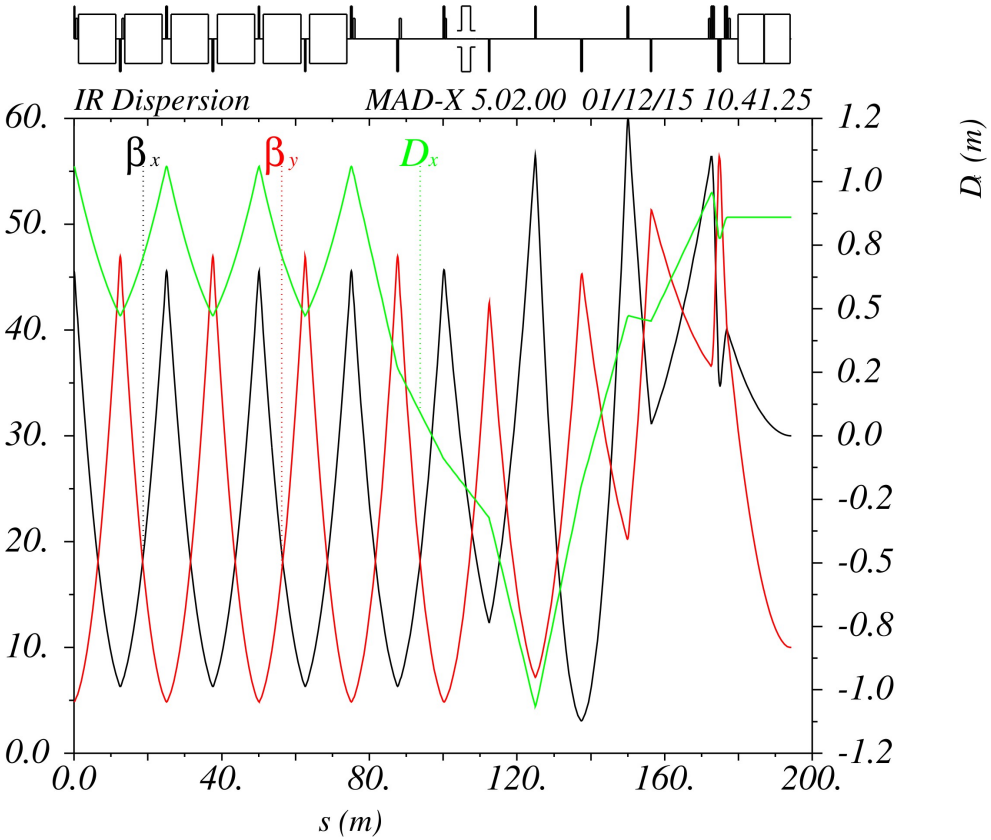


*Figure 15: The high energy configuration. The RW is off.*

# The Ring

The ring consists of 6 ARCs and 6 straight sections described previously. Note, there is freedom to shuffle these straight sections to different IPs. Table 5 shows the ring properties using MADX [6]. The optics for the ring are shown in Figs. 16-18 for the three energy configurations.

The emittance which depends on the radiation integrals varies with the momentum spread. The damping partition number changes with momentum as [2]:

$$\frac{\Delta \mathcal{D}}{\delta} = \frac{2\int K^2 \eta^2 ds}{\oint ds/\rho^2}$$

where $K$ is the quadrupole strength, $\eta$ is the dispersion, $\rho$ is the bending radius of the dipole magnets, $s$ is the position along the beam trajectory and $\delta$ is the momentum spread. Note, $\Delta\mathcal{D}/\delta$ increases as the horizontal phase advance of the cell decreases. Thus, the change of emittance with momentum spread becomes larger in the low energy configuration.

Figs. 19-21 shows the momentum dependence of the emittance for the three energy configuration. The low energy configuration has a pole due to the shift in damping parameter from the RW. Whether this causes a problems for the luminosity needs to be determined.

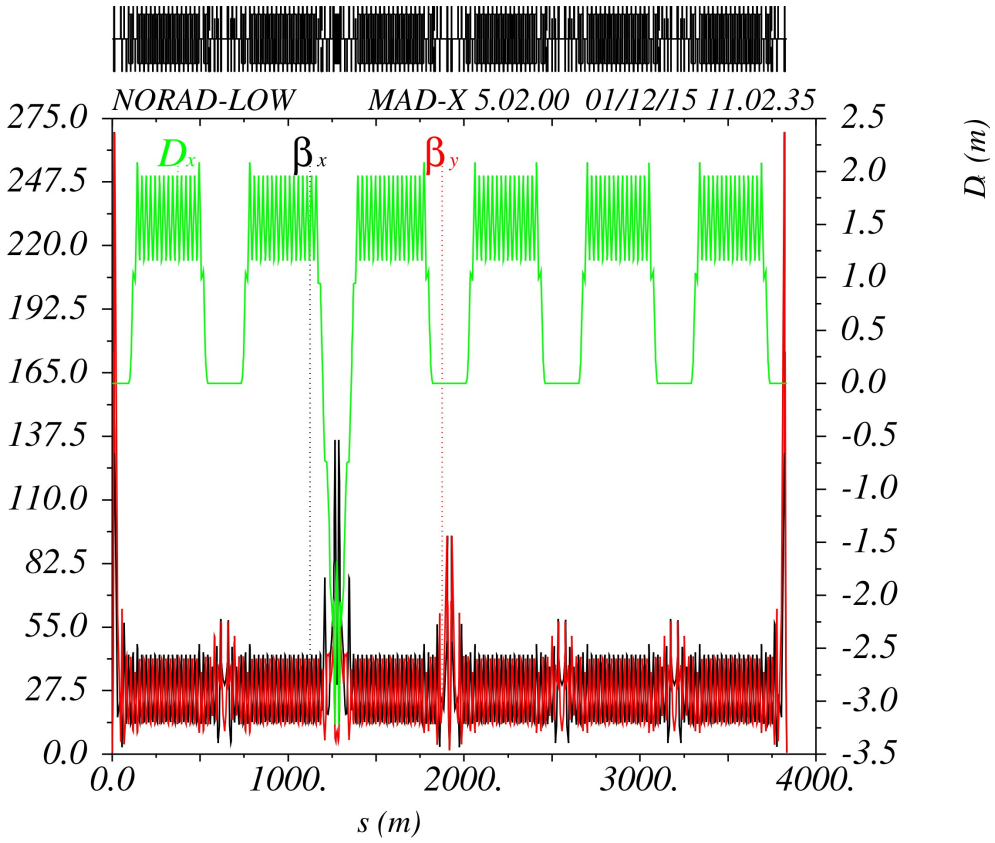


*Figure 16: The ring in the low energy configuration.*

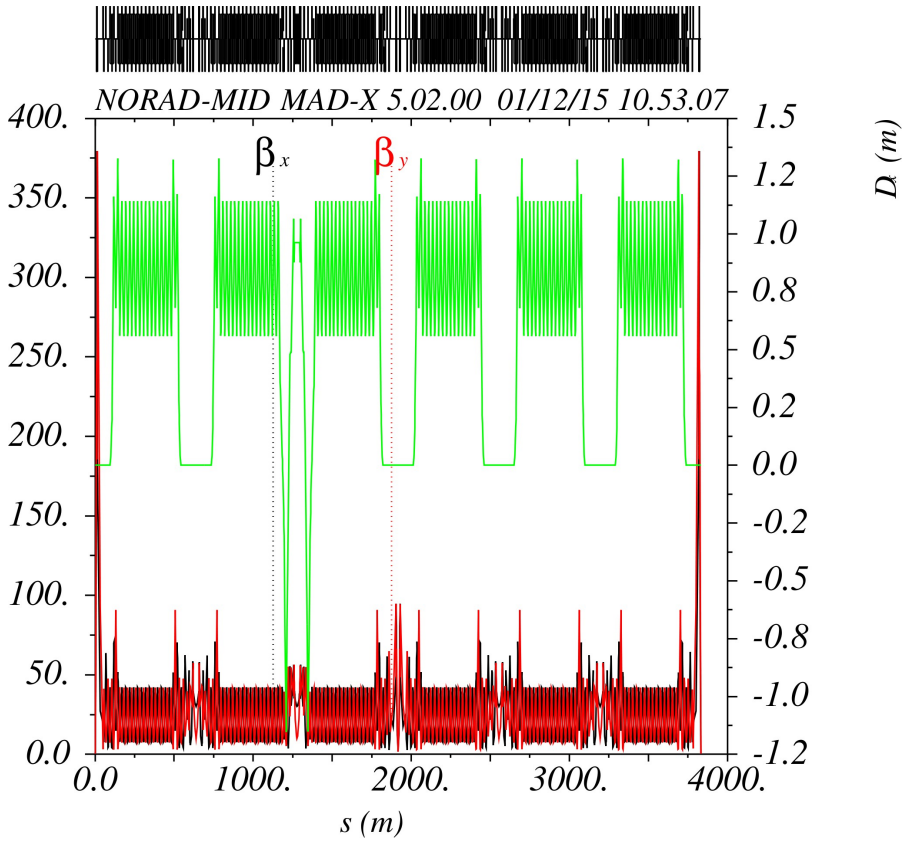


*Figure 17: The ring in the middle energy configuration.*

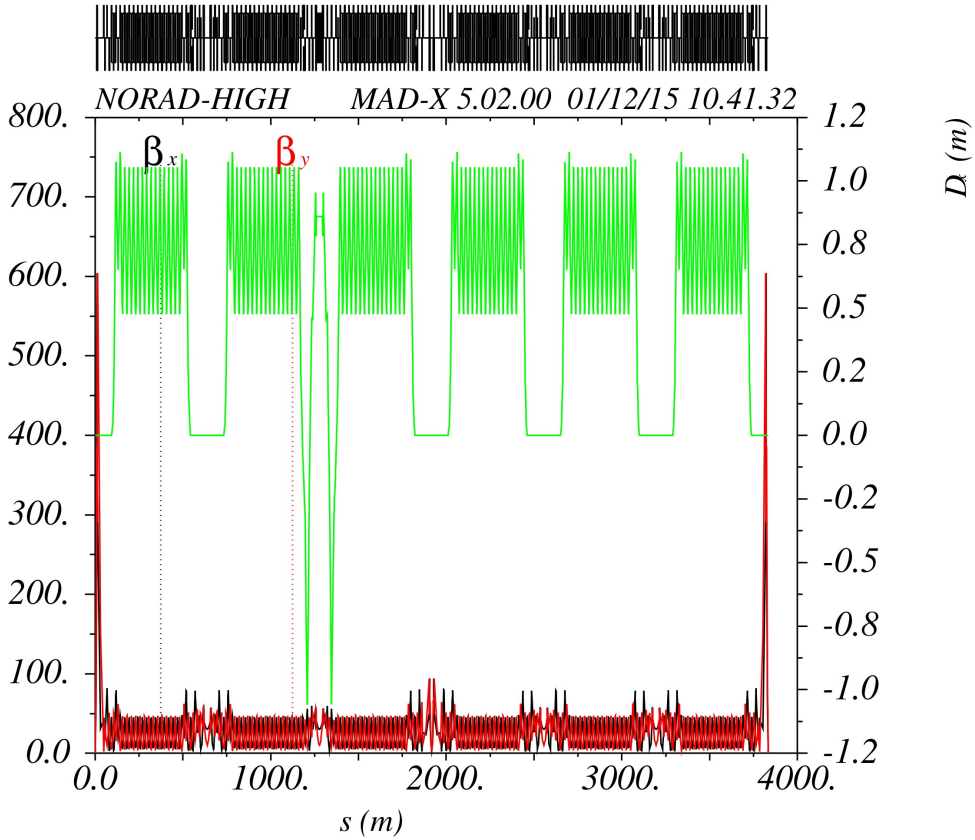


*Figure 18: The ring in the high energy configuration.*

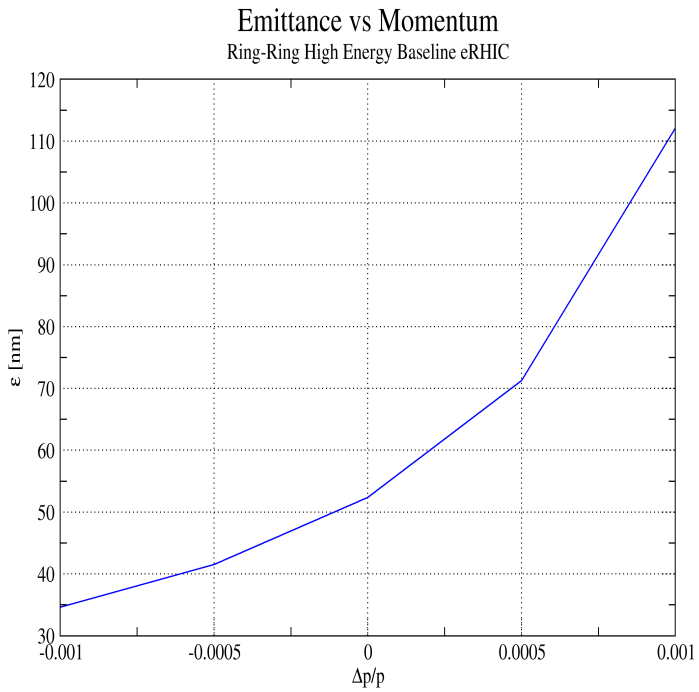


*Figure 19: Emittance versus momentum spread for the high energy configuration. $\Delta D/\delta \approx 520$*

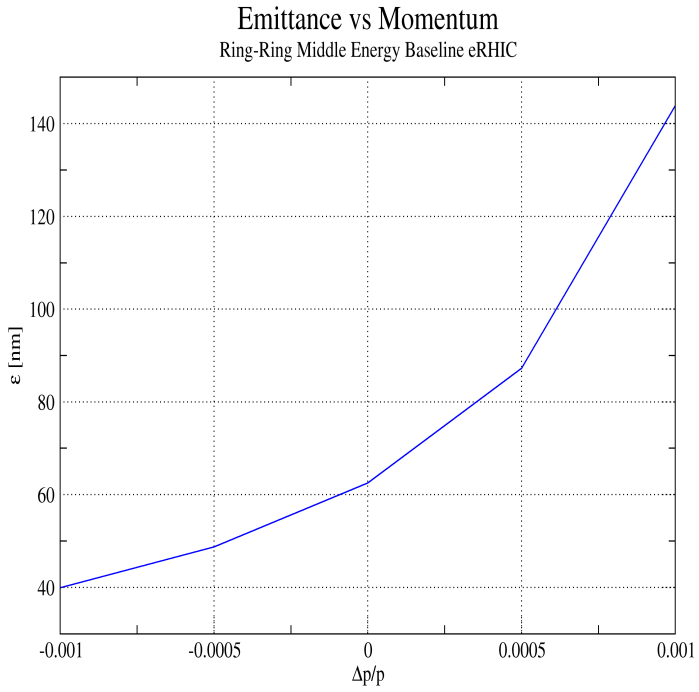


*Figure 20: Emittance versus momentum spread for the middle energy configuration. $\Delta D/\delta \approx 560$*

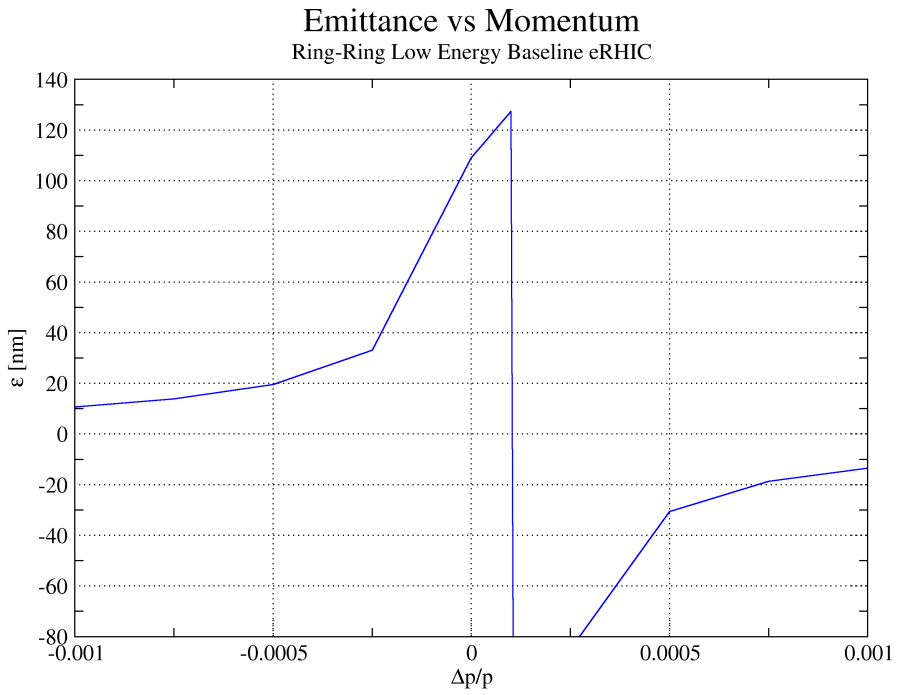


*Figure 21: Emittance versus momentum spread for the low energy configuration. $\Delta\mathcal{D}/\delta \approx 911$. Note, the pole for 0.0001 = Δp/p. This is due in part to using the Robinson Wiggler to shift the damping partition number to, $\mathcal{D}=0.9003$.*

# Conclusion

A design for the electron storage ring to be used in the Ring-Ring eRHIC project is proposed. This ring must fit in the existing RHIC tunnel and have its IP points match the existing IP points of RHIC. This initial design has enough space to be able to use the existing PEP II quadrupoles [4]. Further work needed to be done:

1. Check the rings geometry to the existing RHIC for any conflicts.
2. Redesign with the PEP II quadrupoles.
3. Extend the two families of sextupoles for correction of higher chromatic and amplitude dependent tune effects.
4. Design for real RF cavities, instead of the six RF cavities used.
5. Add additional devices such as BPMs, orbit correctors, spin rotators, wigglers, etc.
6. Beam tracking studies for dynamic aperture, polarization preservation, momentum dependence and beam-beam luminosity.
7. Can we use this ARC design for future upgrade(s)?

| Configuration | Low | Middle | High |
|---|---|---|---|
| **Energy [GeV]** | 5 | 20 | 20 |
| **Design Tunes** | 28.72, 29.82 | 38.28, 39.18 | 40.28, 41.18 |
| **Cell Phase Adv [°]** | 61.76, 65.23 | 88.06, 91.37 | 95.07, 111.82 |
| **Cell Length [m]** | 25.047651 | | |
| **Dipole Length [m]** | 10.123825 | | |
| **ρ [m]** | 309.361304 | | |
| **Circumference [m]** | 3833.845181 | | |
| **Momentum Compaction** | 0.00231 | 0.00123 | 0.00110 |
| **Natural Chrom** | -45.375, -43.148 | -66.414, -67.209 | -80.293, -76.710 |
| **Horizontal Chrom** | 1.83, 140.4, 46738 | 1.86, 359.5, 83866 | 1.85, 725.9, 673201 |
| **Vertical Chrom** | 1.88, 129.9, 26794 | 1.90, 186.6, 11078 | 1.88, -2030.2, 884622 |
| **$\alpha_{xx}$, $\alpha_{xy}$ or $\alpha_{yx}$, $\alpha_{yy}$** | -272.3, -850.5, -165.3 | 37.35, -2315, 32.52 | 4661, 3748, 3348 |
| **$\beta_{max}$ [m]** | 269.1 | 379.4 | 603.8 |
| **Horizontal ε [nm]** | 109.3 | 62.52 | 52.37 |
| **$J_x$** | 0.0994339 | 0.99509099 | 0.99512338 |
| **$J_E$** | 2.90063429 | 2.00490632 | 2.00487382 |
| **$U_0$ [MeV/turn]** | 0.187 | 45.755 | 45.754 |
| **Beam Current [Amp]** | 0.925 | 0.508 | 0.508 |
| **Total SR power [MW]** | 0.173 | 23.243 | 23.243 |

*Table 5: Parameters for the ring in the three energy configurations of the baseline design. The "Design Tunes", "Cell Phase Adv" and "Natural Chrom" rows give the "horizontal, vertical" values. The "Horizontal Chrom" and "Vertical Chrom" rows show the "1st order, 2nd order, 3rd order" chromaticity values from PTC in MADX with two families of sextupoles in the cells. The column "$\alpha_{xx}$, $\alpha_{xy}$ or $\alpha_{yx}$, $\alpha_{yy}$" gives the amplitude dependent tune effects due to the sextupoles. The high energy configuration has very strong chromatic effects which can be reduced by setting the vertical tune to 39.18 (below the horizontal tune).*

# Acknowledgments

We'd like to thank Scott Berg, Vadim Ptitsyn and Dejan Trbojevic for many useful discussions.

## Bibliography

[1] E.C. Aschenauer, S. Berg, M. Blaskiewicz, M. Brennan, A. Fedotov, W. Fischer, V. Litvinenko,C. Montag (chair), R. Palmer, B. Parker, S. Peggs, V. Ptitsyn, V. Ranjbar, S. Tepikian, D. Trbojevic, F. Willeke, *Report of the eRHIC Ring-Ring Working Group*, eRHIC/46 (2015).
[2] S. Y. Lee, *Accelerator Physics*, World Scientific (1999).
[3] R. Ropert, *Low Emittance Lattices*, CERN 95-06, 147-166 (1995).
[4] *PEP-II Conceptual Design Report*, SLAC-418 (1993)
[5] Mario Conte, William W. MacKay, *An Introduction to the Physics of Particle Accelerators*, World Scientific (2008).
[6] *The MADX Program*, http://mad.home.cern.ch/mad, MAD-X 5.02.00 (2014)